Combustion and Flame xxx (xxxx) xxx

Contents lists available at ScienceDirect

Combustion and Flame

journal homepage: www.elsevier.com/locate/combustflame

Low- and intermediate-temperature oxidation of dimethyl ether up to 100 atm in a supercritical pressure jet-stirred reactor

Chao Yan[a], Hao Zhao[a,*], Ziyu Wang[a,*], Guohui Song[a], Ying Lin[a], Clayton R. Mulvihill[b], Ahren W. Jasper[b], Stephen J. Klippenstein[b], Yiguang Ju[a]

[a] Department of Mechanical and Aerospace Engineering, Princeton University, Princeton, NJ 08544, USA
[b] Chemical Sciences and Engineering Division, Argonne National Laboratory, Lemont, IL 60439, USA

ARTICLE INFO

Article history:
Received 12 October 2021
Revised 13 February 2022
Accepted 13 February 2022
Available online xxx

Keywords:
Dimethyl ether
Ultra-high pressure
Jet-stirred reactor
SP-JSR
Low-temperature chemistry

ABSTRACT

Understanding the low- and intermediate-temperature oxidation chemistry of oxygenated fuels like dimethyl ether (DME) at high pressure is paramount to the development of advanced engines with low carbon emissions. The supercritical pressure jet-stirred reactor (SP-JSR) recently developed at Princeton provides a new platform for conducting kinetic studies at low and intermediate temperatures at extremely high pressures with a uniform temperature distribution and a short flow residence time. This paper uses the SP-JSR to investigate DME oxidation at equivalence ratios of 0.175, 1.0, and 1.72, for pressures of 10 and 100 atm, and temperatures ranging from 400 to 900 K. The results demonstrate weakened NTC behavior at 100 atm relative to 10 atm due to increased flux through QOOH + O_2 = O_2QOOH relative to QOOH = 2 CH_2O + OH at 100 atm. Furthermore, the intermediate-temperature oxidation window is shifted to lower temperatures at 100 atm. The experimental data are compared with several chemical kinetic models from the literature. The existing models are seen to agree quite well with the experimental data at 10 atm. However, the models fail to properly capture the NTC behavior at 100 atm. Reaction pathway analyses indicate that both the low- and intermediate-temperature chemistries are controlled by RO_2 consumption pathways. The reaction rates for several of the important reactions, such as DME + OH = CH_3OCH_2 + H_2O, H_2O_2 (+M) = 2 OH (+M), and 2 HO_2 = 2 OH + O_2 are updated in this work. The updated model improves the predictability for all key species compared to the original model.

1. Introduction

High-pressure and supercritical combustion applications have enormous potential for gas turbines and advanced engines, with the supercritical CO_2 cycle providing both higher efficiency and lower CO_2 and soot formation [1–4]. Under extremely high-pressure conditions, multiple-body collisions begin to cause significant deviations in the rate constants from those derived in the isolated binary collisions model that underlies most gas phase kinetics modeling. As a result, the reaction rates may have unusual pressure dependencies for the transition from gas-phase to supercritical conditions. Reaction rates, even for some well-calculated or measured reactions like CO + OH = CO_2 + H, H + O_2 (+M) = HO_2 (+M), and H + O_2 = OH + O, might have significant discrepancies between supercritical and gas-phase conditions. Furthermore, thermodynamic properties, such as entropy and enthalpy, may deviate significantly from the ideal gas law at high pressures. As such, kinetics experiments and theoretical calculations at ultra-high pressures (above 100 atm) are necessary for understanding supercritical combustion chemistry

To explore high-pressure combustion kinetics, Shao et al [5]. recently studied the effect of supercritical CO_2 on fuel ignition through measurements of the ignition delay times of methane and hydrogen highly diluted in CO_2 at 300 bar. Kogekar et al [6]. studied the impact of real-gas considerations on the ignition delay time of *n*-dodecane in a high-pressure shock tube. Liang et al [3]. evaluated the effects of thermodynamic and transport properties on hydrogen and methane flame speed measurements at supercritical conditions. They found that laminar flame speeds at high pressures increase due to the non-ideal equation of state. Hashemi et al [7–9]. used a high-pressure laminar flow reactor to study the supercritical oxidation chemistries of methane, ethane, and propane at 100 bar. Fernandes et al [10]. used a high-pressure flow reactor to perform elementary reaction rate measurements up to 1000 bar.

Unfortunately, only a few research apparatuses in the field of combustion, such as the shock tube [5,6] and high-pressure

* Corresponding authors.
E-mail addresses: cgsq725525@gmail.com (H. Zhao), ziyuw@princeton.edu (Z. Wang).

https://doi.org/10.1016/j.combustflame.2022.112059
0010-2180/

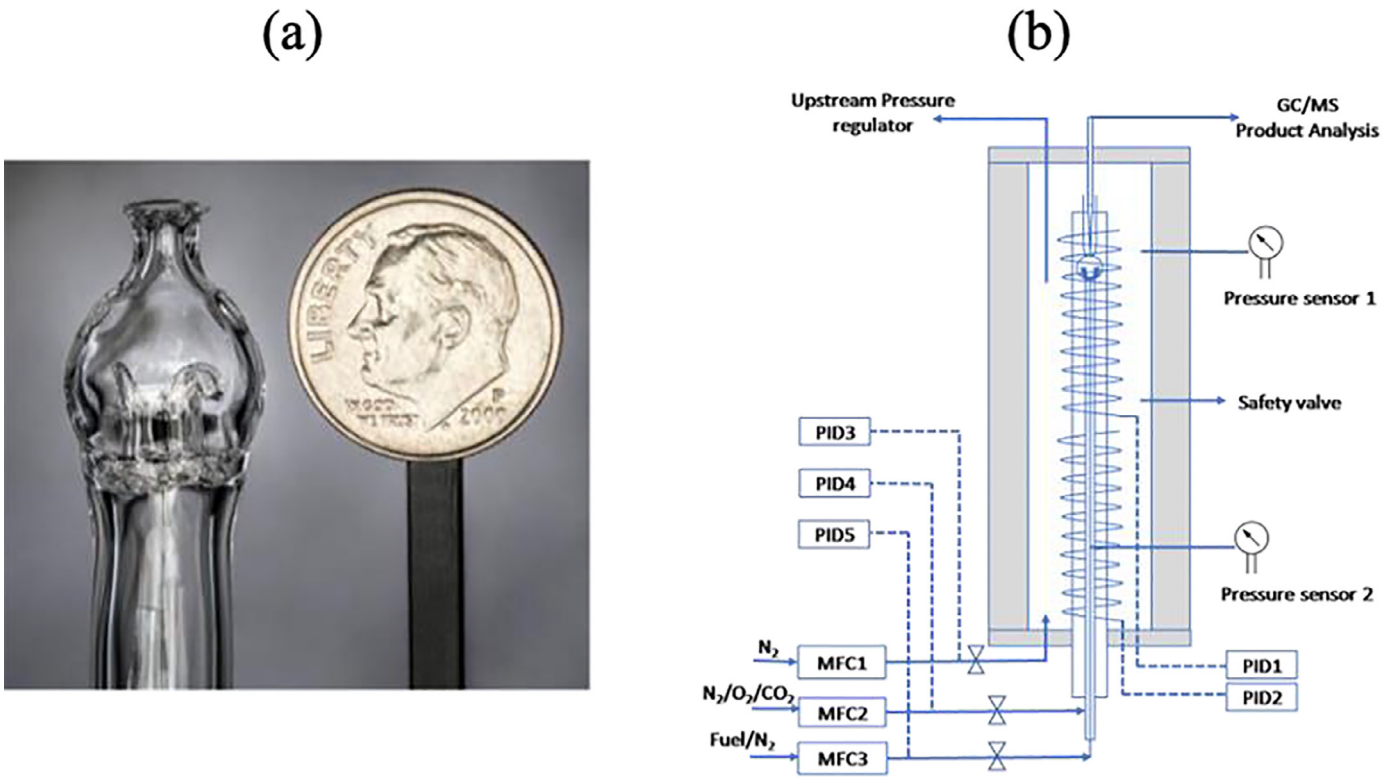

Fig. 1. (a) The quartz part of the reactor; (b) Schematic of the SP-JSR setup.

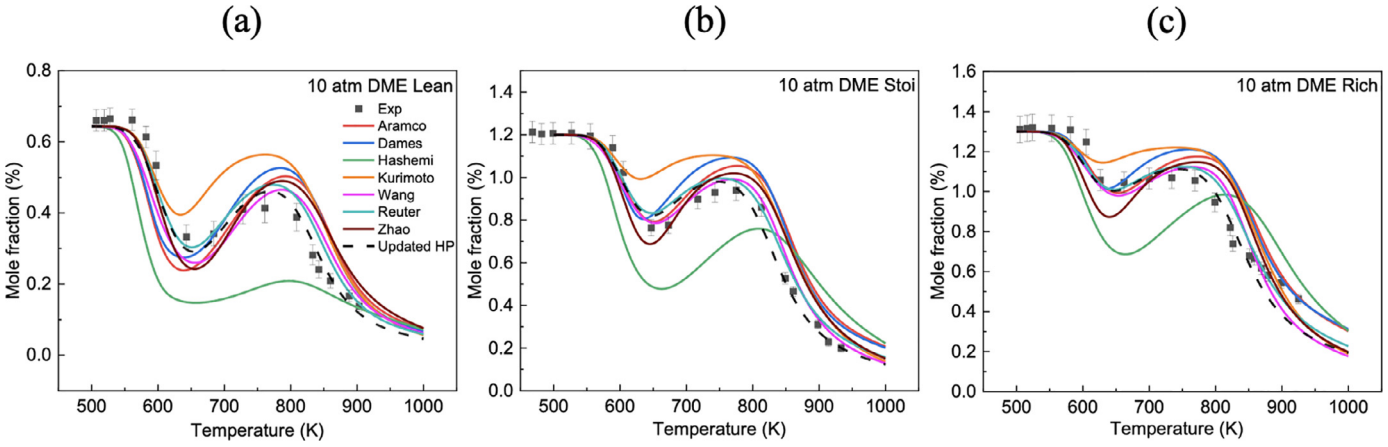

Fig. 2. Temperature evolutions of DME oxidation: (a) lean condition, (b) stoichiometric condition, (c) rich condition; with residence times of 0.12–0.07 s at a pressure of 10 atm.

laminar flow reactor [7–10], can be used to study supercritical reaction chemistry. While modern shock tubes can achieve post-reflected-shock pressures of 250 atm or higher [11], their relatively short test times (typically 10–20 ms) usually constrain them to moderate or high temperatures, where the chemistry is rapid enough. Furthermore, wide-ranging speciation measurements are often challenging. Thus, shock tubes are generally not suited for studying low-temperature (< 800 K) chemistry. Meanwhile, high-pressure laminar flow reactors facilitate numerous speciation measurements, but for the current setups [7–9] the residence time is so long (above 10 s) that the fuel concentration has to be very low in order to slow down the reactivity. This limitation inhibits the observation of negative temperature coefficient (NTC) behavior. While the flow reactor has a lengthy uniform (+/−5 K) temperature regime, it also includes a ramping up and down of the temperature by about 300 K, which can complicate the kinetic modeling. Interestingly, although the flow is laminar, it can be well modeled in the plug flow approximation [12]. An alternative high-pressure jet-stirred apparatus for supercritical kinetics study could provide a valuable complement to shock tubes and flow reactors.

Jet-stirred reactors (JSRs) have been widely used as chemical reactors for the development and validation of detailed chemical mechanisms of fuels [13–15]. Recently, we developed a novel supercritical-pressure jet-stirred reactor (SP-JSR) with operating pressure between 10 and 200 atm and temperature between 300 and 1200 K. It allows for the study of supercritical combustion chemistry [16] over a broad range of temperatures and pressures. The SP-JSR possesses a uniform temperature distribution and a

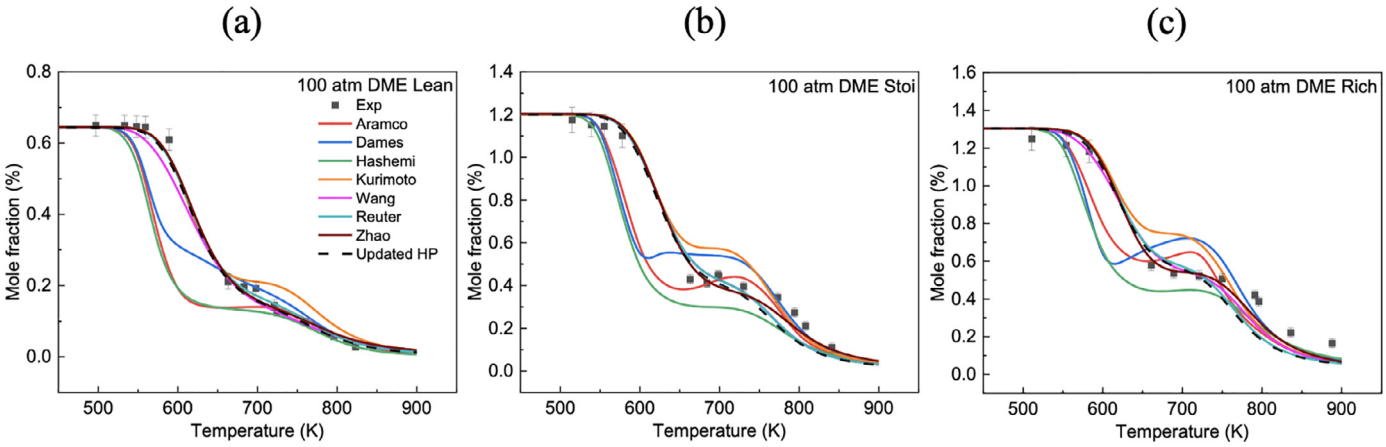

Fig. 3. Temperature evolutions of DME oxidation: (a) lean condition, (b) stoichiometric condition, (c) rich condition; with residence times of 0.44–0.20 s at a pressure of 100 atm.

Table 1
Recent experimental studies performed in jet-stirred reactors and flow reactors.

Equipment type	Temperature (K)	Pressure (atm)	φ	τ (s)	References
JSR	800–1300	1–10	0.2–2	0.1	[26]
JSR	550–1100	1	0.2–1	0.1	[27]
JSR	800–1300	1–10	0.2–2.5		[28]
JSR	540	10	0.35	5	[29]
JSR	550–1100	1	0.25–2	2	[30]
Flow Reactor	490–750	1	0.6	107	[17]
Flow Reactor	500–1150	1	0.2–1.6	0.19–2	[18]
Flow Reactor	1080–1086	1	0.5	0.1	[25]
Flow Reactor	500–1150	1	1	1.5	[31]
Flow Reactor	450–900	50, 100	0.06–20		[32]

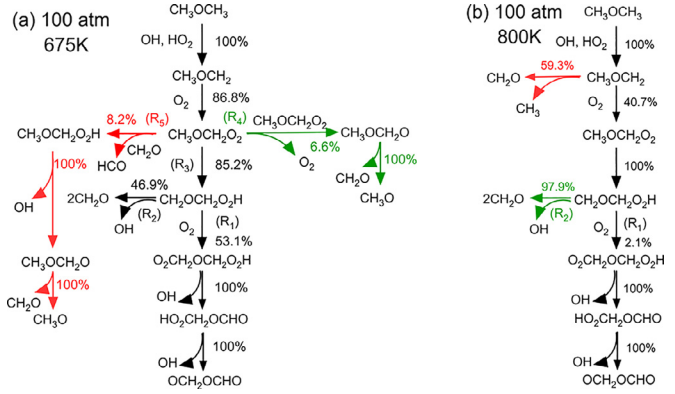

Fig. 4. Reaction pathways for DME at 675 K (a) and 800 K (b) at 100 atm for the rich mixture using the updated HP-Mech model. The thickness of arrows here represents the relative importance of different reaction pathways based on the rate of species production.

well-defined flow residence time ranging from 0.1 to 1 s. We have recently used this SP-JSR to study low and intermediate temperature *n*-butane chemistry at 100 atm [16]. The results clearly showed that there is an NTC effect for *n*-butane at high pressure, although the increase of pressure does weaken the NTC effect.

Dimethyl ether (DME) has been widely investigated as an alternative fuel in diesel and HCCI engines, gas turbines, and fuel cells. As the simplest fuel exhibiting two-stage oxidation behavior, it has been widely used as a model fuel to study the mechanism for low-temperature oxidation [17,18] and cool flames [19,20]. Several models describing the oxidation of DME have been developed based on experimental studies of ignition delays [22–24], species profiles in JSRs [26–30] and flow reactors [17,18,21,25,31,32], and flame measurements [33–35] Table 1. lists the recent experimental studies of DME oxidation performed in JSRs and flow reactors. Notably, recent flow reactor [18] and JSR [29] experiments have shown that all these mechanisms could possibly over-predict DME consumption and HO_2 and H_2O_2 formation at low temperatures [17].

High-pressure (above 40 bar) experimental data remain lacking for DME model validation. Therefore, in this study, we observed DME oxidation at 10 and 100 atm in the SP-JSR and compared our experimental data with several existing kinetic models. In addition to varying the experimental pressure, the equivalence ratio is also varied, with values of 0.175, 1, and 1.72. The temperature is varied between 400 and 900 K. The mole fractions of DME, O_2, CO, CO_2, CH_2O, H_2O, and CH_3OCHO are quantified with a micro-gas chromatograph (μ-GC). The oxidation chemistry of DME is analyzed with an update of several key elementary reactions for radical branching and termination, and important reaction pathways at high pressure are identified.

2. Experimental methods and kinetic models

The SP-JSR is a sphere with an internal volume of 0.4 cm^3. The novelty of the SP-JSR lies in its eight perpendicular nozzles with 0.2 mm inner diameter on four jet fingers at the center of the sphere, which generate intense turbulence and homogenous mixing [36]. Figure 1(a) shows the quartz part of the reactor. The quartz reactor is placed inside a stainless-steel, pressure-resistant jacket. By balancing the pressure inside and outside the reactor, high-pressure working conditions are possible. The gases issuing from the JSR exit are sampled by a quartz sonic nozzle and then equilibrate their pressure with vacuum generated by a dry pump. The experimental system was designed for experiments over the 10–200 atm and 295–1200 K temperature range. The schematic

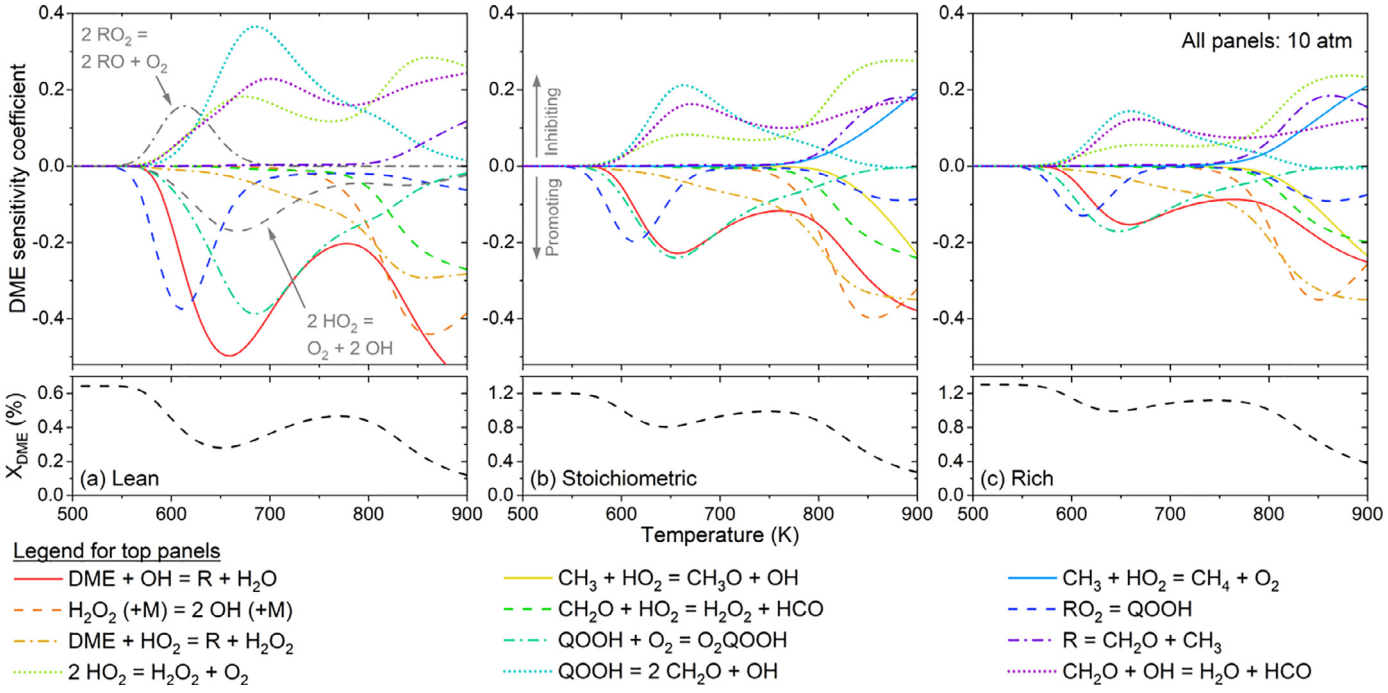

Fig. 5. DME sensitivity coefficients (top panels) and predicted mole fractions (bottom panels) versus temperature for (a) lean, (b) stoichiometric, and (c) rich conditions at the 10-atm conditions of the present study. Simulations were performed in 5-K increments using the updated HP-Mech model. For mixture information, see Table 2. The 12 reactions with the largest magnitudes of S_i for each equivalence ratio between 500 and 900 K are plotted.

Table 2
Experimental conditions.

Case	Equivalence ratio	Pressure (atm)	DME (%)	O_2(%)	N_2 (%)	Residence time (s)	Temperature (K)
1	0.175	10	0.644	11.090	88.266	0.12–0.07	500–900
2	1	10	1.203	3.609	95.188	0.12–0.07	500–900
3	1.72	10	1.303	2.270	96.427	0.12–0.07	500–900
4	0.175	100	0.644	11.090	88.266	0.44–0.20	400–900
5	1	100	1.203	3.609	95.188	0.44–0.20	400–900
6	1.72	100	1.303	2.270	96.427	0.44–0.20	400–900

of the setup is shown in Fig. 1(b), and the detailed description is in [16]. The gas flow rates were controlled by high-pressure mass flow controllers (Brooks, SLA5800) and gas samples were quantified by using a micro gas chromatography (μ-GC) [37]. Two segments of electric heating wires were installed inside the high-pressure shell and three were installed outside. Over a three meters long heating zone, all reactant mixture was completely pre-heated before injection into the JSR bulb. The axial temperature profiles under the experimental flow conditions were measured in 1-mm steps along the JSR bulb, where the temperature variation was within ± 3 K between 400 and 1000 K. The details of the temperature profile measurement are provided elsewhere in [16]. The velocity distribution profile of the reactor cross view is shown in Fig. S1 in Supplemental Information (SI).

The oxidation experiment is conducted under the conditions in Table 2 at 10 and 100 atm between 400 and 900 K. The flow residence time is defined as the ratio of the volume of the reactor to the volume flow rate at the specific temperature and pressure condition. It should be noted that instead of keeping the flow residence time constant, in this experiment the flow residence time of the experiment changes with the temperature to keep a fixed inlet volume flow rate at 1.2 L/min (Cases 1–3) and 4 L/min (Cases 4–6) at 295 K and 1 atm to reduce the error in flow control and perturbation. Moreover, the residence time is chosen to correspond with the oxidation reaction timescale (near unity Damköhler number). We performed the perfect stirred reactor simulation using CHEMKIN software for different residence times. The fuel oxidation profile is very sensitive to the residence time when it is close to the oxidation reaction timscale which we selected in our experiments. Every measurement is repeated at least two times at the same temperature condition Table 2. lists the experimental operating conditions. We used the following eight models to compare to the experimental measurements obtained in the SP-JSR: Zhao et al [21]., Kurimoto et al [18]., Reuter et al. (HP-Mech) [34], Hashemi et al [32]., AramcoMech 2.0 [22], Wang et al [31]., and Dames et al [24].. The updated reaction rates in Reuter et al. (updated HP-Mech) model are listed in Table 3. The real gas effect for DME oxidation at 100 bar is small and can be neglected. Figure S2 in Supplemental Information (SI) shows the comparison of real gas results and ideal gas results. All simulations were performed using the perfect stirred reactor module (fix gas temperature) using the CHEMKIN software, except for the sensitivity analysis, which was performed in the Cantera software [38].

3. Results and discussion

Figure 2 depicts the DME mole fraction evolution against temperature for fuel-lean (Case 1), stoichiometric (Case 2), and fuel-rich (Case 3) conditions with residence times of 0.12–0.07 s at 10 atm. The experimental data exhibit a typical window of NTC behavior from 650 to 775 K. By comparing to the 1-atm experimental data of Wang et al [31]., one can note that the NTC behavior is slightly suppressed at 10 atm compared to that at 1 atm. NTC at normal pressure is due to a competition between

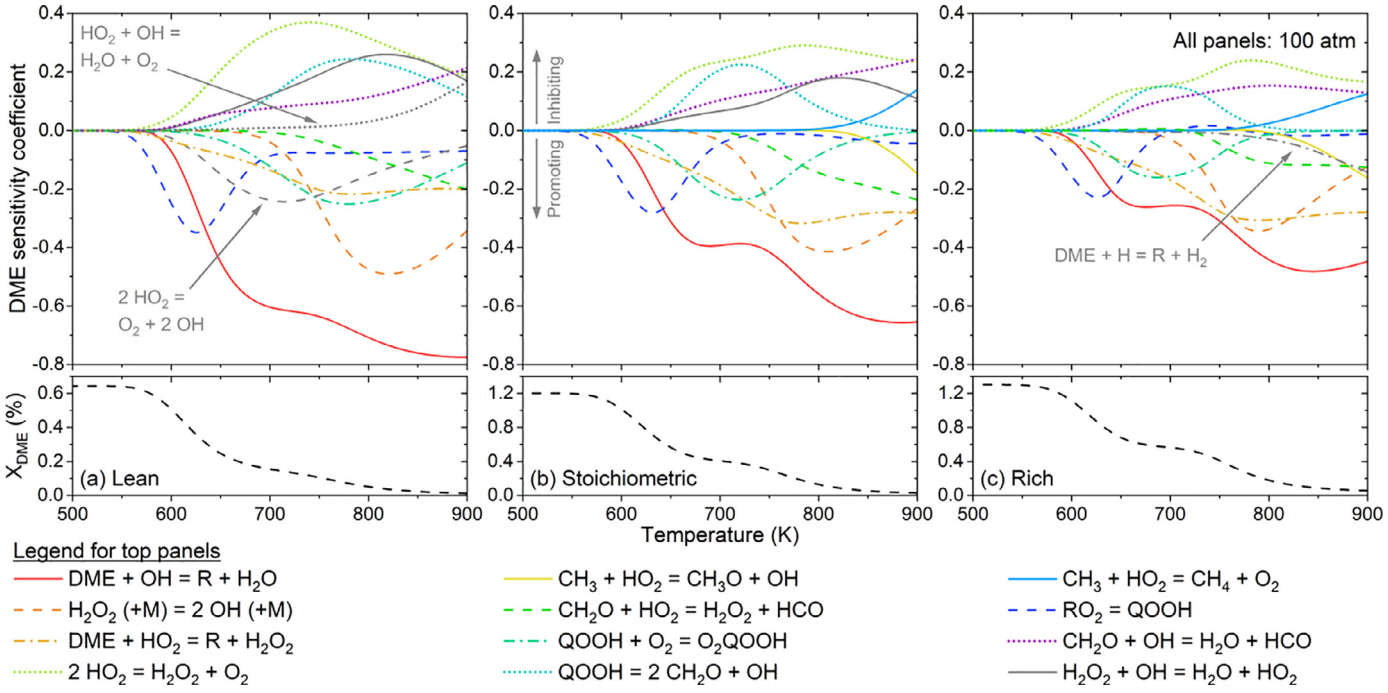

Fig. 6. DME sensitivity coefficients (top panels) and predicted mole fractions (bottom panels) versus temperature for (a) lean, (b) stoichiometric, and (c) rich conditions at the 100-atm conditions of the present study. Simulations were performed in 5-K increments using the updated HP-Mech model. For mixture information, see Table 2. The 12 reactions with the largest values of S_i for each equivalence ratio between 500 and 900 K are plotted. With the exception of the reaction $H_2O_2 + OH = H_2O + HO_2$, the reactions in the legend are the same as those in the 10-atm case (Fig. 5).

Table 3
Updated reaction rates in Reuter (HP-Mech) model.

Reactions	A ($cm^3/mol.s$)	n	Ea (cal/mol)	Ref.
$CH_3OCH_3+OH<=>CH_3OCH_2+H_2O$	2.32E+05	2.467	−1040	[39]
$H+O_2<=>O+OH$	7.26E+14	−0.235	15,928.7	[40]
$OH+OH<=>O+H_2O$	9.32E+03	2.564	−2603.7	[40]
$H+H+H_2<=>H_2+H_2$	1.02E+17	−0.6	0	[40]
$H+OH(+M)<=>H_2O(+M)$	2.51E+13	0.234	−114	[40]
LOW	4.50E+25	−3.064	1581.4	
TROE	0.72	1.0E-30	1.0E+30	
$H+O_2(+M)<=>HO_2(+M)$	1.03E+12	0.604	−241.1	[40]
LOW	1.74E+19	−1.23	0	
TROE	0.495	1.0E-30	1.0E+30	
$HO_2+OH<=>O_2+H_2O$	7.44E+12	0.055	−915.2	[40]
DUP	1.17E+23	−2.156	23,681	
$HO_2+HO_2<=>H_2O_2+O_2$	1.93E-02	4.12	−4960	[41]
$HO_2+HO_2<=>OH+OH+O_2$	6.41E+17	−1.54	8540	[41]
$H_2O_2+H<=>H_2+HO_2$	4.40E+01	3.45	712	[40]
$H_2O_2+H<=>H_2O+OH$	3.35E+07	1.91	3654	[40]
$H_2O_2(+M)<=>2OH(+M)$	2.00E+12	0.9	48,749	[40]
LOW	2.49E+24	−2.3	48,749	
TROE	0.43	1.0E-30	1.0E+30	
$HO_2CH_2OCHO<=>OCH_2OCHO + OH$				[42]
1.00E-02	1.95E+89	−23.59	63,890.0	
1.00E-01	2.39E+77	−19.55	61,350.0	
1.00E+00	1.65E+60	−13.95	56,580.0	
1.00E+01	1.82E+42	−8.20	51,040.0	
1.00E+02	2.44E+29	−4.12	46,860.0	

two channels ($QOOH+O_2$ and QOOH decomposition). However, at high pressure, not only the low-temperature chemistry is proportional to $[O_2]^n$ (n = 1–2) [43], but also the radical production via $H_2O_2+(M)=2OH+(M)$ and $2HO_2=2OH+O_2$ reactions is dramatically increased and shifted to lower temperature Therefore, with an increase in pressure, both the low-temperature oxidation rate increases nonlinearly and the HO_2 chemistry, which suppresses the NTC effect via QOOH and O_2QOOH decomposition. Moreover, it can be noted that the initiation temperature of low-temperature oxidation is around 550 K, which is unusual for such a small fuel molecule (e.g., n-alkanes). This can be explained by the presence of an O-atom that weakens the neighboring C–H bond, favoring the H-abstractions compared with similar n-alkanes [30]. As to the model simulation at 10 atm, all models slightly over-predict the DME oxidation at the very beginning. The updated HP-Mech model (black dash lines) yields very good agreement with the experimental data for temperatures of 600–900 K at these conditions. Additionally, the Zhao et al., Reuter et al., and Wang et al. models all predict the experimental data reasonably well. The Hashemi et al. and Aramco models over-predict DME oxidation in the

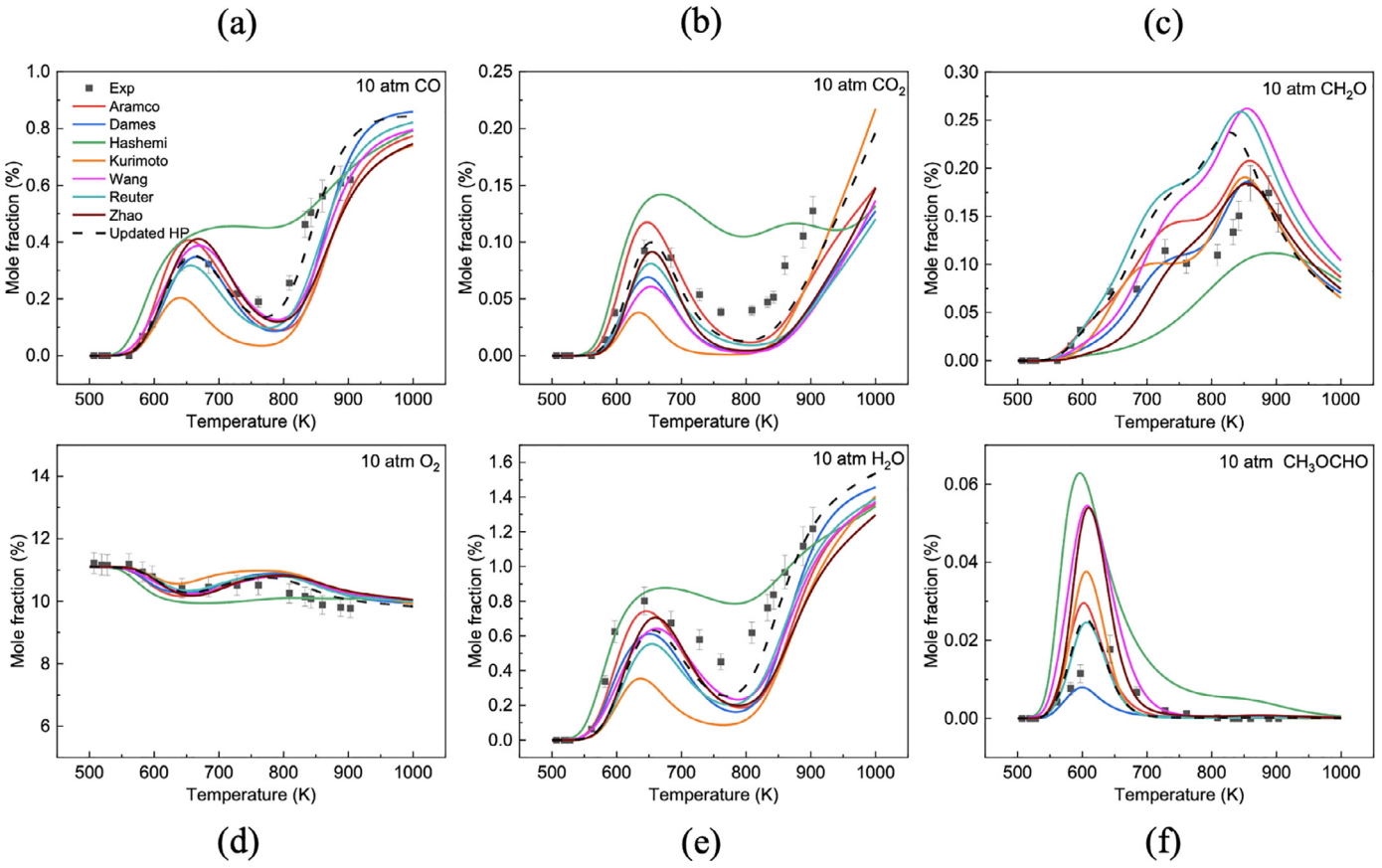

Fig. 7. Temperature evolutions of the mole fraction of CO (a), CO_2 (b), CH_2O (c), O_2 (d), H_2O (e), and CH_3OCHO (f) for the fuel lean condition (Case 1) from 500 to 900 K at 10 atm.

low-temperature region, while the Kurimoto et al. and Dames et al. models under-predict DME oxidation in the NTC region. The good agreement between experimental data and simulation results at 10 atm reveals that the SP-JSR can reproduce the results at 10 atm pressure for kinetic model validation and could provide more useful experimental results for model validation under extreme pressures.

Figure 3 depicts the DME mole fraction evolution against temperature for fuel-lean (Case 4), stoichiometric (Case 5), and fuel-rich (Case 6) conditions with flow residence times of 0.44–0.20 s at 100 atm. It should be mentioned that the flow residence times of 100 atm are slightly longer than 10 atm and the difference would result in slightly more reactivity at 100 atm condition. This small difference will only slightly affect the starting point of fuel oxidation; however, it doesn't affect other phenomenon (e.g., NTC behavior). It is seen that this high-pressure experimental data also exhibits a typical window of NTC behavior from 650 to 725 K. However, compared to the results at 10 atm, the NTC behavior is greatly suppressed at 100 atm. In addition, the low-and intermediate-temperature oxidation onset temperature increases slightly with pressure. This is because of the nonlinear increase of the low temperature reactivity with the oxygen concentration or pressure $\omega_{LTC} \sim [O_2]^n \sim [p]^n$ (n=1–2) [43]. In comparing the model predictions with the experimental data at 100 atm, the updated HP-Mech, Zhao et al., Reuter et al., and Wang et al. models predict the experimental data at these three conditions reasonably well, especially with regard to the NTC behavior. The Hashemi et al. and Aramco models over-predict the DME oxidation both at low and intermediate temperatures, while the Kurimoto et al. and Dames et al. models under-predict the DME oxidation in the NTC region. It is interesting to note that some existing models over-predict the DME oxidation even at atmospheric pressures [17,18]. However, overall, their performance becomes better at the higher pressures of the present study. In our previous study of *n*-butane [16] and propane oxidations [44] at 100 atm and lower pressures [16], model predictions captured the NTC behavior of *n*-butane and propane accurately at low pressures while under-predicting their oxidation at 100 atm. The contrasting predictions of the low-temperature oxidation of DME, *n*-butane, and propane imply that there exist large discrepancies in pressure-dependent fuel oxidation in their low-temperature chemistry. More information provided in SI (Figure S3) shows the temperature evolution of the fuel mole fraction of *n*-butane as an example.

Based on the model performance at 10 and 100 atm, the updated HP-Mech model was selected to investigate the detailed kinetics of DME oxidation. To this end, a reaction pathway analysis was performed at 675 and 800 K and 100 atm for the rich mixture of the present study; the respective results are shown in Fig. 4(a) and (b). The reaction pathway analysis of 10 atm is shown in SI Fig. S4. Figure 4 illustrates that the low-temperature chemistry of DME follows the well-known chain-branching mechanisms for hydrocarbons. The fuel radical CH_3OCH_2 (R) is formed via H abstraction reactions from DME (RH) mainly by OH and HO_2 radicals. The first O_2 addition produces $CH_3OCH_2O_2$ (RO_2), which can isomerize to form a carbon-centered radical, $CH_2OCH_2O_2H$ (QOOH). The fate of QOOH is in large part controlled by the competition between the second O_2 addition, QOOH + O_2 = $O_2CH_2OCH_2O_2H$ (O_2QOOH) (R1), and thermal dissociation, QOOH = $2CH_2O$ + OH (R2). This competition for QOOH largely mediates the NTC behavior of DME (another aspect of the NTC region is the competition between DME and CH_2O to consume OH radicals; see the discussion on the sensitivity plots below). The O_2QOOH can then isomerize

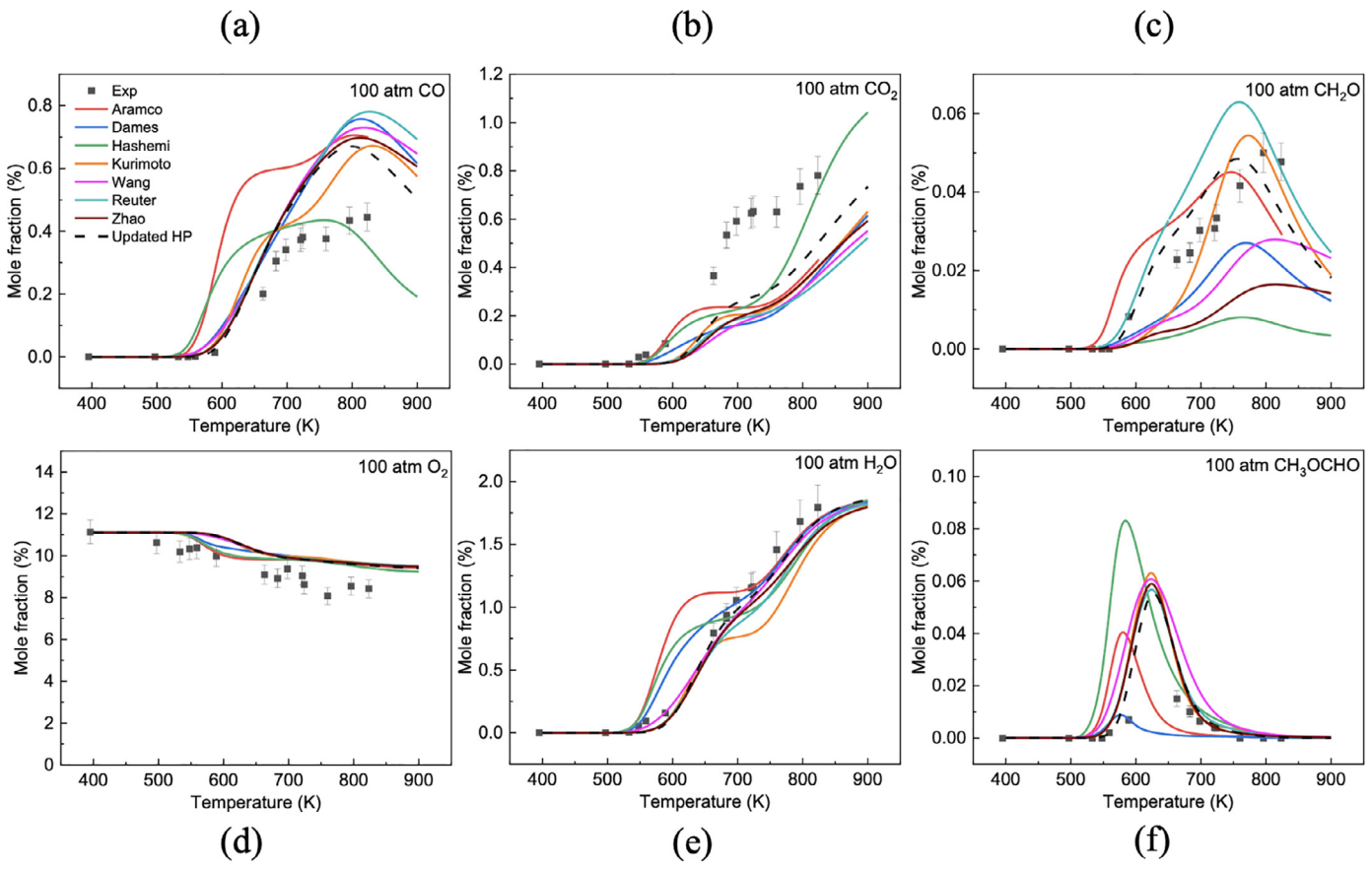

Fig. 8. Temperature evolutions of the mole fraction of CO (a), CO_2 (b), CH_2O (c), O_2 (d), H_2O (e), and CH_3OCHO (f) for the fuel lean condition (Case 4) from 400 to 900 K at 100 atm.

and rapidly decompose to form an OH radical and a ketohydroperoxide, HO_2CH_2OCHO (KHP). The KHP can decompose to produce another OH and a keto-alkoxy radical, OCH_2OCHO (OQ'O), thereby completing the chain-branching process.

In addition to the main chain-branching pathway described above, other pathways compete for RO_2 radicals. The self-reaction of RO_2, 2 RO_2 = 2 CH_3OCH_2O (RO) + O_2 (R4), yields two sets of CH_2O and CH_3O [see Fig. 4(a)]. Additionally, the pathway through the reaction RO_2 + CH_2O = $CH_3OCH_2O_2H$ + HCO (R5) has a net yield of HCO, OH, CH_2O, and CH_3O [see Fig. 4(a)]. The competition of the chain-inhibiting R4 with RO_2 = QOOH (R3) is important to DME oxidation at low temperatures. At 800 K in Fig. 4(b), the direct dissociation of R begins to compete with the O_2 addition pathway, reducing the production of RO_2.

Although not illustrated in Fig. 4, the H-abstraction reaction from DME by HO_2 has a significant impact on the oxidation at high pressures and high temperatures (above ~800 K), while its importance is minor compared to DME + OH at low pressures and low temperatures (below ~800 K). This change in importance is because HO_2 production at high pressure increases dramatically, and reactions involving HO_2 then have a higher impact on the fuel oxidation. We believe that one of the major uncertainties in the variation in the model simulations with pressures comes from the DME + HO_2 reaction, which could benefit from a high-level ab initio kinetics analysis. A varying role for non-thermal reactions, as discussed in our recent study of diethyl ether oxidation [42], may also play a key role in interpreting the dependence on pressure.

To further investigate the low-temperature oxidation chemistry of DME, a sensitivity analysis was performed for DME concentrations at both 10 and 100 atm. In contrast to typical sensitivity analyses, the calculations were performed over a fine grid of temperatures, as reported in our recent work [42], to provide a smoothly varying picture of the sensitivity coefficients versus temperature. The normalized, first-order DME sensitivity coefficient for the i-th reaction, S_i, is defined as $S_i = (A_i/X_{DME})(\partial X_{DME}/\partial A_i)$, where A_i is the pre-exponential factor for the i-th rate constant and X_{DME} is the DME mole fraction.

The 10-atm sensitivity analysis is presented in the top panels of Fig. 5 for the three mixtures investigated herein (the bottom panels of Fig. 5 display the predicted DME mole fractions for visual reference). The observations that can be drawn from these plots are many, and only a few will be summarized here. The oxidation onset region (550–600 K) is primarily sensitive to the competition for RO_2 radicals between R3 and R4 (R4 is in competition with R3 in all three panels of Fig. 5 but appears only in Fig. 5(a) due to the plotting truncation to 12 reactions). As the temperature increases into the NTC region, the opposing sensitivities to R1 and R2 become large as these reactions compete for QOOH. With the temperature increasing further beyond the NTC region, thermal dissociation of R becomes increasingly rapid and the reverse reaction RO_2 = R + O_2 increases in importance; both of these effects inhibit the low-temperature chain-branching mechanism. Concurrently, the importance of the HO_2 radical grows, with the sensitivity to DME + HO_2 growing near the peak of the NTC region (~775 K in all three panels of Fig. 5) along with sensitivity to H_2O_2 = 2 OH (H_2O_2 is mainly formed via HO_2 + HO_2 = H_2O_2 + O_2).

The reaction 2 HO_2 = O_2 + 2 OH shows up in the fuel-lean panels of Fig. 5 (it is not shown in the stoichiometric and fuel-rich panels due to the plotting truncation). This reaction occurs via singlet HO_2 and was recently explored for the first time [41]; this rate constant was part of the updates to the updated HP-Mech (see the

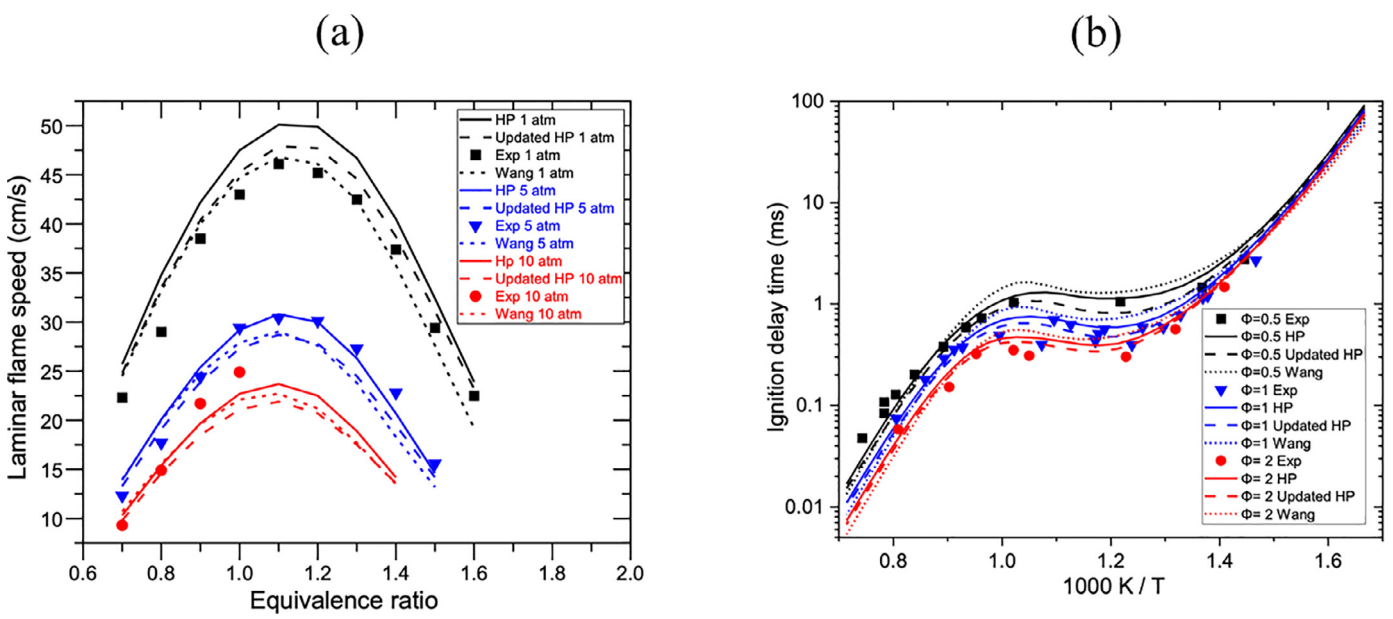

Fig. 9. Comparison of experimental and simulated (updated HP-Mech and Wang et al. models) results for (a) laminar flame speeds of DME/air mixtures with different equivalence ratios at pressures of 1, 5, and 10 atm [45] and (b) ignition delay times of DME/air mixtures with different equivalence ratios at 25 atm, except for the fuel-rich data, which were obtained at 15 atm [22].

Supporting Information). Not surprisingly, this chain-propagating (or chain-branching) reaction has an opposite sign from the chain-terminating reaction 2 $HO_2 = H_2O_2 + O_2$.

In all three panels of Fig. 5, the chain-propagating reaction DME + OH = R + H_2O has one of the largest sensitivity coefficients. The significant dip in sensitivity to this reaction across the NTC region occurs partly due to the increased formation of CH_2O via QOOH decomposition; the CH_2O competes with DME for consumption of OH radicals.

The changes in the DME sensitivity coefficients with equivalence ratio are somewhat subtle. With increasing equivalence ratio, the sensitivities to QOOH + O_2 = O_2QOOH (R1) and QOOH = 2 CH_2O + OH (R2) become ~0 at lower temperatures [e.g., they are both ~0 by ~875 K in Fig. 5(b), while they are both ~0 by ~850 K in Fig. 5(c)]. Lower [O_2] inhibits both the first and second O_2 additions. Another subtle change due to equivalence ratio is the importance of R decomposition, R = CH_2O + CH_3. In Fig. 5(a–c), the peak sensitivity to this reaction shifts to lower temperatures as the equivalence ratio is increased. This increased sensitivity to R decomposition occurs due to less consumption of R via R + O_2 = RO_2 with decreasing [O_2].

DME sensitivity coefficients at 100 atm are shown in Fig. 6. As was observed in the experimental data, the difference between the 10- and 100-atm cases is quite significant. This difference is perhaps most marked by the shape of the sensitivity to DME + OH, which almost completely lacks the dip in the NTC region that was observed in the 10-atm case [cf Fig. 5(a)]. The explanation for this difference is as follows. The bimolecular nature of QOOH + O_2 = O_2QOOH (R1) greatly promotes the flux through this pathway at higher pressures, whereas the competing reaction QOOH = 2 CH_2O + OH (R2) is unimolecular and assumed to be pressure independent in the updated HP-mech. Therefore, increasing pressure greatly favors O_2QOOH formation over QOOH decomposition. A reaction pathway analysis on the rich mixture at 10 atm and 675 K indicated that 67% of the QOOH proceeds through the beta-scission pathway (R2), while 29% proceeds through the second O_2 addition (R1). However, at 100 atm (and 675 K), the situation is nearly inverted: only 35% of the QOOH flux is via R2, with 63% going through R1. It is because of the suppression of R2 in favor of R1 that inhibits the NTC behavior at 100 atm relative to 10 atm. It is noted in Fig. 6 that at 100 atm OH production from H_2O_2 + (M) = 2 OH + (M) and $2HO_2$ = 2 OH + O_2 is dramatically increased and shifted to lower temperature. The enhanced HO_2 branching channel suppresses the NTC effect with the increase of temperature. Although the flux through R2 is greatly reduced at 100 atm relative to 10 atm, the R2 sensitivity coefficient at 100 atm in Fig. 6(c) is still comparable to that of R1; the added insight from the pathway analysis highlights the benefit of employing both sensitivity and reaction pathway analyses. The reduced flux through decomposition of QOOH concomitantly reduces the formation of CH_2O. Since, as mentioned previously, CH_2O competes with DME to consume OH radicals, the suppressed NTC behavior leads to less of a dip in the DME + OH sensitivity. Another factor that slightly reduces CH_2O formation is the increased consumption of R to form RO_2 at higher pressure, which impedes R from decomposing to form CH_2O + CH_3. For this reason, R decomposition does not appear in the top 12 reactions of Fig. 6, while it did appear at all three equivalence ratios in Fig. 5.

A notable absence from the sensitivity analyses (Figs. 5 and 6) is KHP decomposition, KHP = OQ'O + OH. Presumably, this absence is because KHP decomposition is rapid enough to not be a "bottleneck" in the chain-branching process. However, there is one detail worth mentioning. Some of us have recently applied variable reaction coordinate transition state theory to calculate the analogous rate constant in the diethyl ether system [42]. The rate constant obtained from these calculations was 1–2 orders of magnitude slower than values in the literature. Indeed, the KHP decomposition rate constant employed in the HP-Mech is over 10 times larger than the analogous rate constant calculated in the diethyl ether system in [42]. Therefore, the KHP decomposition rate constant has been modified in the updated HP-Mech model. It slightly modifies the onset temperature of the oxidation; however, the difference is very small.

Figure 7(a)–(f) shows the mole fractions of other important species at 10 atm, such as CO, CO_2, CH_2O, O_2, H_2O, and CH_3OCHO, respectively. It can be noted that the updated HP-Mech model improves the predictions for all key species compared to the original model. The modeling slightly underpredicts CO_2 and H_2O forma-

tion and overpredicts CH_2O and CH_3OCHO formations. The species profiles in Fig. 7 demonstrate NTC behavior in the same region as the DME mole fraction profile. Therefore, the agreement between experimental and modeling data is satisfactory and they are cross validated for the 10-atm conditions.

Figure 8(a)–(f) shows the mole fractions of other important species at 100 atm, such as CO, CO_2, CH_2O, O_2, H_2O, and CH_3OCHO, respectively. The NTC behavior for the species in Fig. 8 is much weaker compared to that in Fig. 7, which is consistent with the temperature evolution of DME mole fractions. The modeling results underpredict CO_2 formation and overpredict CO and CH_3OCHO formations. It can also be noted that the discrepancy between experimental and numerical simulation results for CO and CO_2 production are still noticeable at temperatures higher than 700 K. Therefore, the reaction rates of HOCO = CO + OH, HOCO = CO_2 + H, CO_2 + OH = CO + HO_2, and CO_2 + H = CO + OH need careful evaluation at supercritical conditions.

4. Comparison with literature data

In this section, we further validate the updated HP-Mech model against two sets of experimental data from the literature: laminar flame speeds [45] and ignition delay times [22] of DME/air mixtures. Comparisons are also made with the previous HP-Mech [34] and Wang et al. models [31] Figure 9(a) shows experimental laminar flame speed data for different equivalence ratios at different pressures [46]. Simulations were performed for an initial gas temperature of 298 K and at initial pressures of 1, 5, and 10 atm. In general, the agreement between experimental and modeling data is satisfactory at different equivalence ratios, although the model slightly overpredicts the laminar flame speed at a pressure of 1 atm and underpredicts the laminar flame speed at pressures of 5 and 10 atm Figure 9(b) shows the ignition delay time data with different equivalence ratios of 0.5–2.0 and 25 atm [22]. The comparison covers both the low- and intermediate-temperature regions. Although the model slightly overestimates the ignition delay time in the low-temperature region, the NTC behavior is well reproduced. Ignition delay times calculated using the updated HP-Mech model in general show good agreement with the experimental data for all equivalence ratios. The comparison of the updated HP-Mech model and jet-stirred reactor data in literature is shown in Fig. S5.

5. Conclusions

The novel supercritical pressure jet stirred reactor (SP-JSR) provides a valuable platform for conducting kinetic studies at low and intermediate temperatures at extreme pressures under a uniform temperature distribution and a short flow residence time. The low and intermediate temperatures of DME oxidation have been investigated using the SP-JSR at equivalences ratios of 0.175, 1.0, and 1.72, pressures of 10 and 100 atm, and temperatures from 400 to 900 K. The experiments show that a weaker NTC behavior is observed at 100 atm compared to 10 atm.

Seven existing models and one updated model were compared to the experimental measurements made by the SP-JSR. The updated model has the best agreement with the new SP-JSR experimental data among these models. The Zhao et al., Reuter et al., and Wang et al. models predict the experimental data at these three conditions reasonably well, especially in capturing the NTC behavior. The Hashemi et al. and Aramco models over-predict DME oxidation both at low and intermediate temperatures, while the Kurimoto et al. model and Dames et al. model under-predict DME oxidation in the NTC region at 100 atm.

Reaction pathways and sensitivity analyses show that both low- and intermediate-temperature chemistries are dominated by the typical chain-branching mechanism for hydrocarbons at both 10 and 100 atm. At normal pressure, the competing reactions of QOOH + O_2 = O_2QOOH (R1) and QOOH = 2CH_2O + OH (R2) control the NTC behavior. However, the NTC behavior is largely suppressed at 100 atm due to the favoring of R1 over R2 with increasing pressure and the increased radical production rate at lower temperature via H_2O_2 + (M) = 2 OH + (M) and 2 HO_2 = 2 OH + O_2 reactions. The discrepancy between experimental and modeling data of minor species at 100 atm implies that the reaction rates of HOCO = CO + OH, HOCO = CO_2 + H, CO_2 + OH = CO + HO_2, and CO_2 + H = CO + OH need to be further considered at supercritical conditions.

Declaration of Competing Interest

We declare that we have no financial and personal relationships with other people or organizations that can inappropriately influence our work, there is no professional or other personal interest of any nature or kind in any product, service and/or company that could be construed as influencing the position presented in, or the review of, the manuscript entitled.

Hao Zhao

Mechanical Aerospace Engineering Department, Princeton University

10/10/2021

Acknowledgements

YJ would like to sincerely thank Prof. Katherina Kohse-Höinghaus for her long-time support and collaborations in combustion chemistry. We would like to present this work to honor her great contributions to combustion chemistry and to remember our collaboration on dimethyl ether chemistry. This work was partly supported by ARO grant W911NF-16–1–0076 and the DOE BES award DE-SC0021135. The material in this study is based in part on work at ANL supported by the U.S. Department of Energy (USDOE), Office of Basic Energy Sciences, Division of Chemical Sciences, Geosciences, and Biosciences under DOE Contract Number DE-AC02–06CH11357 through the Argonne-Sandia Consortium on High-Pressure Combustion Chemistry, FWP 59044.

Supplementary materials

Supplementary material associated with this article can be found, in the online version, at doi:10.1016/j.combustflame.2022.112059.

References

[1] R.D. Reitz, Combustion and ignition chemistry in internal combustion engines, Int. J. Engine Res. 14 (2013) 411–415.
[2] G.P. Sutton, O. Biblarz, Rocket propulsion elements, John Wiley & Sons, 2016.
[3] W. Liang, W. Li, C.K. Law, Laminar flame propagation in supercritical hydrogen/air and methane/air mixtures, Proc. Combust. Inst. 37 (2019) 1733–1739.
[4] H. Zhao, N. Zhao, C. Yan, Z. Zhang, Y. Ju, Studies of multi-channel spark ignition characteristics of n-pentane/air mixture under fuel lean conditions in a spherical bomb, Combust. Flame 212 (2020) 337–344.
[5] J. Shao, R. Choudhary, D.F. Davidson, R.K. Hanson, S. Barak, S. Vasu, Ignition delay times of methane and hydrogen highly diluted in carbon dioxide at high pressures up to 300bar, Proc. Combust. Inst. 37 (2019) 4555–4562.
[6] G. Kogekar, C. Karakaya, G.J. Liskovich, M.A. Oehlschlaeger, S.C. DeCaluwe, R.J. Kee, Impact of non-ideal behavior on ignition delay and chemical kinetics in high-pressure shock tube reactors, Combust. Flame 189 (2018) 1–11.
[7] H. Hashemi, J.M. Christensen, S. Gersen, H. Levinsky, S.J. Klippenstein, P. Glarborg, High-pressure oxidation of methane, Combust. Flame 172 (2016) 349–364.
[8] H. Hashemi, J.G. Jacobsen, C.T. Rasmussen, J.M. Christensen, P. Glarborg, S. Gersen, M. van Essen, H.B. Levinsky, S.J. Klippenstein, High-pressure oxidation of ethane, Combust. Flame 182 (2017) 150–166.
[9] H. Hashemi, J.M. Christensen, L.B. Harding, S.J. Klippenstein, P. Glarborg, High–pressure oxidation of propane, Proc. Combust. Inst. 37 (2019) 461–468.

[10] R.X. Fernandes, K. Luther, J. Troe, Falloff curves for the reaction $CH_3 + O_2$ (+ M) → CH_3O_2 (+ M) in the pressure range 2-1000bar and the temperature range 300-700K, J. Phys. Chem. A 110 (2006) 4442–4449.
[11] E.L. Petersen, D.F. Davidson, R.K. Hanson, Kinetics modeling of shock-induced ignition in low-dilution CH_4/O_2 mixtures at high pressures and intermediate temperatures, Comb. Flame 117 (1999) 272–290.
[12] C.L. Rasmussen, J. Hansen, P. Marshall, P. Glarborg, Experimental measurements and kinetic modeling of CH_4/O_2 and $CH_4/C_2H_6/O_2$ conversion at high pressure, Int. J. Chem. Kinet. 40 (2008) 454–480.
[13] P. Dagaut, M. Cathonnet, J.P. Rouan, et al., A jet-stirred reactor for kinetic studies of homogeneous gas-phase reactions at pressures up to ten atmospheres (~1MPa), J. Phys. E Sci. Instrum. 19 (1986) 207–209.
[14] H. Zhao, A.G. Dana, Z. Zhang, W.H. Green, Y. Ju, Experimental and modeling study of the mutual oxidation of N-pentane and nitrogen dioxide at low and high temperatures in a jet stirred reactor, Energy 165 (2018) 727–738.
[15] H. Zhao, L. Wu, C. Patrick, Z. Zhang, Y. Rezgui, X. Yang, G. Wysocki, Y. Ju, Studies of low temperature oxidation of n-pentane with nitric oxide addition in a jet stirred reactor, Combust. Flame 197 (2018) 78–87.
[16] H. Zhao, C. Yan, T. Zhang, G. Ma, M. Souza, C. Zhou, Y. Ju, Studies of high-pressure n-butane oxidation with CO_2 dilution up to 100bar using a supercritical–pressure jet-stirred reactor, Proc. Combust. Inst. 38 (2021) 279–287.
[17] H. Guo, W. Sun, F.M. Haas, T. Farouk, F.L. Dryer, Y. Ju, Measurements of H_2O_2 in low temperature dimethyl ether oxidation, Proc. Combust. Inst. 34 (2013) 573–581.
[18] N. Kurimoto, B. Brumfield, X. Yang, T. Wada, P. Diévart, G. Wysocki, Y. Ju, Quantitative measurements of HO_2/H_2O_2 and intermediate species in low and intermediate temperature oxidation of dimethyl ether, Proc. Combust. Inst. 35 (2015) 457–464.
[19] S.H. Won, B. Jiang, P. Diévart, C.H. Sohn, Y. Ju, Self-sustaining n-heptane cool diffusion flames activated by ozone, Proc. Combust. Inst. 35 (2015) 881–888.
[20] Y. Ju, C.B. Reuter, S.H. Won, Numerical simulations of premixed cool flames of dimethyl ether/oxygen mixtures, Combust. Flame 162 (2015) 3580–3588.
[21] Z. Zhao, M. Chaos, A. Kazakov, F.L. Dryer, Thermal decomposition reaction and a comprehensive kinetic model of dimethyl ether, Int. J. Chem. Kinet. 40 (2008) 1–18.
[22] U. Burke, K.P. Somers, et al., An ignition delay and kinetic modeling study of methane, dimethyl ether, and their mixtures at high pressures, Combust. Flame 162 (2015) 315–330.
[23] U. Pfahl, K. Fieweger, G. Adomeit, Self-ignition of diesel-relevant hydrocarbon-air mixtures under engine conditions, Symp. (Int.) Combust. 26 (1996) 781–789.
[24] E.E. Dames, et al., A detailed combined experimental and theoretical study on dimethyl ether/propane blended oxidation, Combust. Flame 168 (2016) 310–330.
[25] S.L. Fischer, F.L. Dryer, H.J. Curran, The reaction kinetics of dimethyl ether. I: high-temperature pyrolysis and oxidation in flow reactors, Int. J. Chem. Kinet. 32 (2000) 713–740.
[26] P. Dagaut, J.C. Boettner, M. Cathonnet, Chemical kinetic study of dimethylether oxidation in a jet stirred reactor from 1 to 10 BAR: experiments and kinetic modeling, Symp. (Int.) Combust. 26 (1996) 627–632.
[27] P. Dagaut, C. Daly, J.S. Simmie, M. Cathonnet, Oxidation and ignition of dimethylether from low to high tTemperature (500−1600K): experiments and kinetic modeling, Symp. (Int.) Combust. 27 (1998) 361–369.
[28] H.J. Curran, W.J. Pitz, C.K. Westbrook, P. Dagaut, J.C. Boettner, M. Cathonnet, A wide range modeling study of dimethyl ether oxidation, Int. J. Chem. Kinet. 30 (1998) 229–241.
[29] K. Moshammer, A.W. Jasper, D.M. Popolan-Vaida, et al., Detection and identification of the keto-hydroperoxide ($HOOCH_2OCHO$) and other intermediates during low-temperature oxidation of dimethyl ether, J. Phys. Chem. A 119 (2015) 7361–7374.
[30] A. Rodriguez, et al., Experimental and modeling investigation of the low-temperature oxidation of dimethyl ether, J. Phys. Chem. A 119 (2015) 7905–7923.
[31] Z. Wang, X. Zhang, L. Xing, L. Zhang, F. Herrmann, K. Moshammer, F. Qi, K. Kohse-Höinghaus, Experimental and kinetic modeling study of the low-and intermediate-temperature oxidation of dimethyl ether, Combust. Flame 162 (2015) 1113–1125.
[32] H. Hashemi, J. Christensen, P. Glarborg, High-pressure pyrolysis and oxidation of DME and DME/CH_4, Combust. Flame 205 (2019) 80–92.
[33] X. Qin, Y. Ju, Measurements of burning velocities of dimethyl ether and air premixed flames at elevated pressures, Proc. Combust. Inst. 30 (2005) 233–240.
[34] C. Reuter, R. Zhang, O. Yehia, Y. Rezgui, Y. Ju, Counterflow flame experiments and chemical kinetic modeling of dimethyl ether/methane mixtures, Combust. Flame 196 (2018) 1–10.
[35] Z. Wang, C. Yan, Y. Lin, M. Zhou, B. Jiang, N. Liu, H. Zhong, Y. Ju, Kinetics and extinction of non-premixed cool and warm flames of dimethyl ether at elevated pressure, Proc. Combust. Inst. (2022) Under Review.
[36] H. Zhao, M. Souza, Y. Ju, A supercritical jet-stirred reactor, Fusion J. Am. Sci. Glassblowers Soc. 66 (2018) 19–24.
[37] H. Zhao, Z. Zhang, Y. Rezgui, N. Zhao, Y. Ju, Studies of high pressure 1,3-butadiene flame speeds and high temperature kinetics using hydrogen and oxygen sensitization, Combust. Flame 200 (2019) 135–141.
[38] D.G. Goodwin, R.L. Speth, H.K. Moffat, B.W. Weber, Cantera: an object-oriented software toolkit for chemical kinetics, thermodynamics, and transport processes, version 2.5.1; Cantera, (2021) DOI: 10.5281/zenodo.4527812.
[39] S.J. Klippenstein, From theoretical reaction dynamics to chemical modeling of combustion, Proc. Combust. Inst. 36 (2017) 77–111.
[40] H. Zhao, C. Yan, Z. Wang, A.W. Jasper, S.J. Klippenstein, Y. Ju, et al., High-pressure hydrogen oxidation in N_2, CO_2, and H_2O dilutions up to 100 atm in a supercritical-pressure jet-stirred reactor, Combust. Flame (2000) (in preparation).
[41] S.J. Klippenstein, R. Sivaramakrishnan, U. Burke, K.P. Somers, H.J. Curran, L. Cai, H. Pitsch, M. Pelucchi, T. Faravelli, P. Glarborg, $HO_2 + HO_2$: high level theory and the role of singlet channels, Combust. Flame (2022) https://doi.org/10.1016/j.combustflame.2021.111975.
[42] C.R. Mulvihill, A.D. Danilack, C.F. Goldsmith, M. Demirea, L. Sheps, Y. Georgievskii, S.N. Elliott, S.J. Klippenstein, Non-Boltzmann effects in chain branching and pathway branching for diethyl ether oxidation, Energy Fuels 35 (2021) 17890–17908.
[43] Y. Ju, Understanding cool flames and warm flames, Proc. Combust. Inst. 38 (2021) 83–119.
[44] H. Zhao, C. Yan, G. Song, Z. Wang, Y. Ju, Studies of low and intermediate temperature oxidation of propane up to 100 atm in a supercritical-pressure jet–stirred reactor, Proc. Combust. Inst. (2022) Under Review.
[45] J. De Vries, W.B. Lowry, Z. Serinyel, H.J. Curran, E.L. Petersen, Laminar flame speed measurements of dimethyl ether in air at pressures up to 10 Atm, Fuel 90 (2011) 331–338.